In Robotics Review 2 1992

A Comparative Analysis of Actuator Technologies for Robotics

Contributed by

John M. Hollerbach
Ian W. Hunter
John Ballantyne

1 Introduction

There has been considerable progress in developing traditional actuator technologies for robotics in the past few years. Nevertheless, if we are to achieve the lightweight, high performance, and mobile robots envisioned for the future, new technologies may be required. New applications such as microrobotics require actuators with bandwidths, dynamic ranges, and forces not achievable in traditional ways. Especially severe packaging problems are presented by force-reflecting masters in telerobotics.

This article analyzes a number of promising new actuator technologies for robotics, including shape memory alloy, piezoelectric, magnetostrictive, and polymeric actuators. A comparison will be made to traditional technologies, including electromagnetic, hydraulic, and pneumatic actuators, as well as to muscle, from standpoints of

- power/mass
- torque/mass or force/mass
- individual characteristics

High power/mass is a general requirement for all robotics. With an increased emphasis on direct-drive robotics, torque/mass becomes

very important. Because of space limitations, other important standpoints could not be adequately addressed, such as bandwidth *vs.* power (Thayer, 1984), maximum acceleration (Pasch and Seering, 1984), and moving mass or inertia *vs.* force or torque (Nakanishi, 1991). A general discussion of desirable actuator characteristics has been presented by Jacobsen *et al.* (1989).

In the following, we first discuss macro-motion actuators, beginning with the more traditional electromagnetic, hydraulic, and pneumatic actuators, then following with shape memory alloy and polymeric actuators. We then discuss piezoelectric and magnetostrictive actuators, which are primarily micro-motion actuators. There follows a section on muscle and a general discussion.

2 Electromagnetic Motors

There is a wide variety of electromagnetic (EM) motors, such as synchronous, induction, and dc motors. Fundamentally they are the same, since torque for rotary motors (to which the subsequent discussion is limited) is generated by the interaction of magnetic fields from the rotor and stator. On one side of the rotor/stator gap these fields are set up by current-carrying coils. On the other side, the magnetic fields may arise from permanent magnets, electromagnets, or induced currents. The torque for a particular EM motor depends on the magnetic field distribution in the airgap between rotor and stator.

For purposes of discussion, we will use the example of a permanent magnet dc motor. The permanent magnets are on the stator; armature windings are on the rotor and are mechanically commutated with brushes. The mechanical and electrical equations are:

$$\tau = K_T i \tag{1}$$

$$V = K_T \omega + Ri \tag{2}$$

where τ is the motor torque, K_T is the torque constant, i is the current, V is the supplied voltage, ω is the rotor speed, $E = K_T\omega$ is the back-emf, and R is the winding resistance. For a fixed voltage V, the torque-speed curves are derived from Equations (1) and (2):

$$\tau = K_T(V - K_T\omega)/R = K_T V/R - K_m^2\omega \tag{3}$$

where the motor constant is $K_m = K_T/\sqrt{R}$ and the slope of the torque-speed curves is $-K_m^2$.

By the conservation of energy, we can write

$$P_{in} = P_{loss} + P_{mech} \tag{4}$$

where $P_{in} = Vi$ is the electrical power delivered by the power supply, $P_{mech} = Ei$ is the mechanical power produced by the motor, and $P_{loss} = i^2R$ is the power lost to ohmic heating. The mechanical power P_{mech} versus speed ω has a parabolic form, and can be derived from (3):

$$P_{mech} = \tau\omega = K_T\omega(V - K_T\omega)/R \tag{5}$$

The maximum velocity is given by $\omega_{max} = V/K_T$, and the maximum mechanical power occurs at $\omega_0 = \omega_{max}/2$, or $(P_{mech})_{max} = (VK_m/2K_T)^2$.

2.1 Characteristics

A motor's torque/mass depends on the EM design, while the power/mass additionally depends on the power electronics. The torque/mass is limited by the gap magnetic flux densities and by the maximum currents that can be sustained for a given period of time. Modern rare-earth permanent magnet materials are not easily demagnetized, meaning that motor currents are typically limited by thermal, not magnetic, considerations. Moreover, such magnets are capable of providing gap flux densities at or near electrical steel magnetic saturation limits for typical slot/tooth geometries. A typical maximum value for B_g, the "effective" gap flux density (*i.e.*, the rms value of the spatial flux distribution around the airgap), is 0.5 T.

The sustainable current depends on the allowable winding temperature T_w, which is usually less than 180 °C and typically 130 °C, and on a motor's thermal resistance R_{therm}, which is the temperature rise in °C per dissipated watt due to ohmic heating. R_{therm}, which depends strongly on the thermal environment, is typically measured with the motor mounted to an aluminum plate in ambient temperature with no forced-air cooling.

The achievable torque depends on the specified "duty cycle": much higher torques can be achieved for short durations than for long or continuous periods. From Equation (3), the peak torque at stall is $\tau_{peak} = K_TV/R$, and hence depends not only on the intrinsic motor design (the term K_T/R) but also on the voltage V delivered by the power supply. A better indication of intrinsic motor performance would be the continuous stall torque τ_{cont}, which can be derived from R_{therm}. The maximum continuously sustainable power lost to ohmic heating is:

$$(P_{loss})_{cont} = (T_w - T_a)/R_{therm} = i_{cont}^2R \tag{6}$$

Parameter	Units	1410-01	1410-02	1410-03	1410-05
K_T	N·m/A	0.2	0.50	0.31	0.26
R	Ω	0.28	1.97	0.71	0.45
K_m	N·m/$\sqrt{\text{W}}$	0.27			
R_{therm}	°C/W	1.16			
T_w	°C	155			
τ_{cont}	N·m	2.89			

Table 1: Specifications for Aerotech Model 1410 dc servo motors. Four different winding configurations are shown.

where T_a is the ambient temperature. Combining with Equation (1),

$$\tau_{cont} = K_T i_{cont} = K_T \sqrt{(P_{loss})_{cont}}/\sqrt{R} = K_m \sqrt{(P_{loss})_{cont}} \quad (7)$$

As an example, specifications for the Aerotech Model 1410 dc servo motor are shown in Table 1. Four different winding configurations are given with different K_T and R values, but with the same K_m and R_{therm} values. This is explained by the fact that when manufacturers offer alternative windings they simply change the number of turns N and substitute a commensurately larger or smaller diameter wire so as to maintain a constant copper "fill factor." Since K_t is proportional to N and R to N^2, K_m remains unchanged. From Table 1 and the equations above, $(P_{loss})_{cont}$ = 112 W and τ_{cont} = 2.86 N·m, which agrees closely with the manufacturer's specification (Table 1).

Because manufacturers do not follow a standard in specifying the operating winding and ambient temperatures and the conditions of thermal transfer under which a motor is tested, it is difficult to compare torque capability from different manufacturers' specifications. To better reflect the physical characteristics of the motor rather than the test conditions, one possibility is to combine the motor constant K_m with the thermal resistance R_{therm} as follows.

The motor constant K_m is virtually independent of motor speed and input current and of how the motor is wound (number of turns), so long as the slot fill (conductor area in a slot) is the same. An example again is provided by the different Aerotech models in Table 1, which have the same K_m but different K_T's. A complicating factor is that K_m is temperature dependent because R is; for example, the winding resistance at a maximum allowable winding temperature of $T_w = 155\,°\text{C}$ is typically about 1.5 times that at ambient temperature $T_a = 25\,°\text{C}$. Thus one would have to distinguish between "cold" and "hot" values

for K_m in manufacturers' specification sheets; if not distinguished, they can usually be calculated from other data. Figure 1(a) plots K_m versus mass for a range of Inland Motor Corp. brushless motors; K_m grows approximately linearly with motor mass, though a diameter dependence is also evident.

The motor constant implies a fundamental fact about motors: to produce torque it is necessary to dissipate power in the windings (see equation (7)). The dissipated power causes heat, which must be transferred away as determined by the thermal/mechanical design of the motor to prevent overheating. This ability to transfer heat is indicated by $1/R_{therm}$ (thermal conductance), which in the case of convective heat transfer is proportional to the external surface area presented by the motor to the surrounding air. The parameter $1/R_{therm}$ is plotted for the same Inland brushless motors in Figure 1(b), but against motor surface area. Since the motor constant indicates how much torque is produced per dissipated watt, and the thermal conductance indicates how many dissipated watts are produced per °C temperature rise, they may be combined as $K_m/\sqrt{R_{therm}}$ to provide a single parameter that indicates the amount of torque that can be continuously sustained for a given winding temperature. The square root of the thermal conductance is used for dimensional matching. A plot of this combined parameter for the same Inland brushless motors is shown in Figure 2. When compared in this manner, seemingly disparate motor designs often end up with about the same torque capability.

2.2 Robotics Applications

2.2.1 Geared Drive Motors

Current motor designs are fairly close to the limits of torque/mass set by the present state of non-superconducting electromagnetics. We demonstrate this with a simple dc motor model. The motor length is l, the rotor radius is r, and the stator outer diameter is D; hence the area of the air gap is $A = 2\pi rl$. Permanent magnets in the stator typically produce an effective field distribution in the gap of $B_g = 0.5$ T rms. Similarly, the rotor is wrapped by a current sheet distribution with a typical effective current per axial length of $i_l = 35,000$ A/m. This figure is not an absolute limit, but is typical of some examples of EM machines of conventional geometry (Say, 1976). From the Lorentz relation (Woodson and Mecher, 1990), the maximum tangential force per unit area of the air gap is given by $dF/dA = i_l B_g$. Hence the total torque is:

$$\tau_{cont} = (dF/dA)Ar = 2\pi r^2 l i_l B_g \tag{8}$$

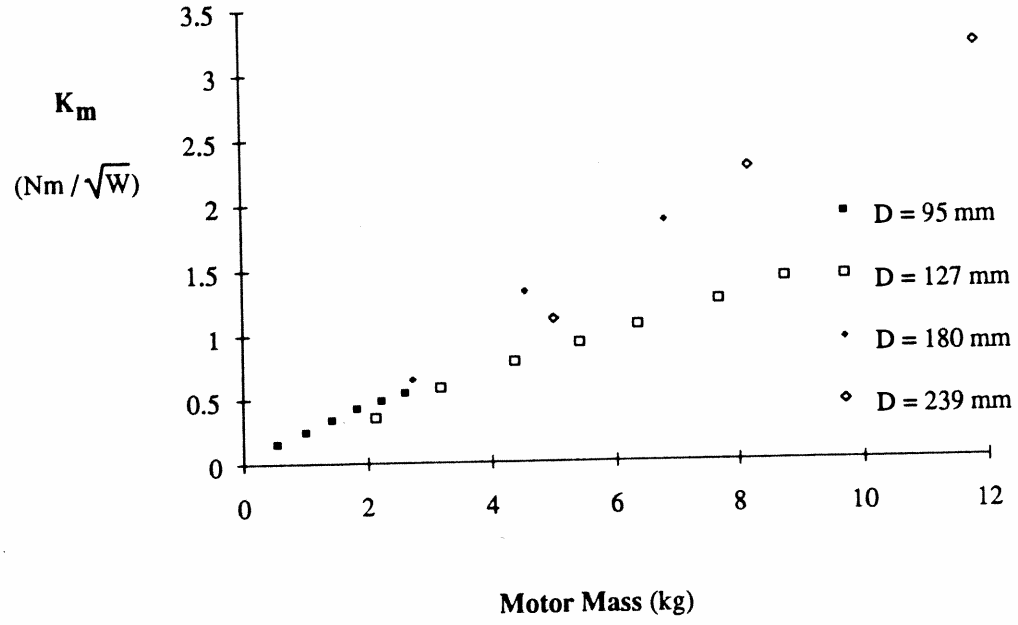

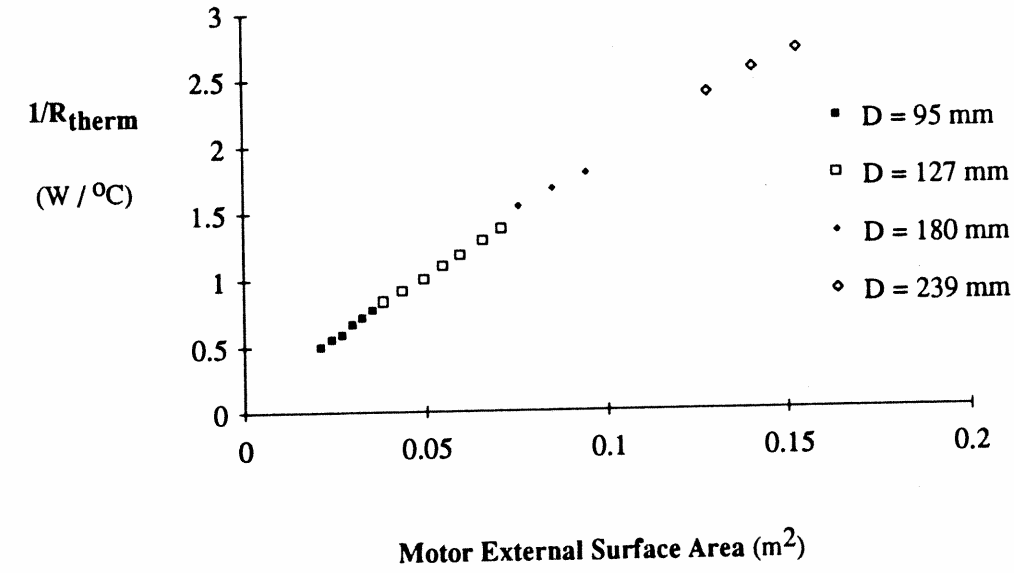

Figure 1: (a) K_m *vs.* motor mass for Inland brushless motors. (b) $1/R_{therm}$ *vs.* motor surface area.

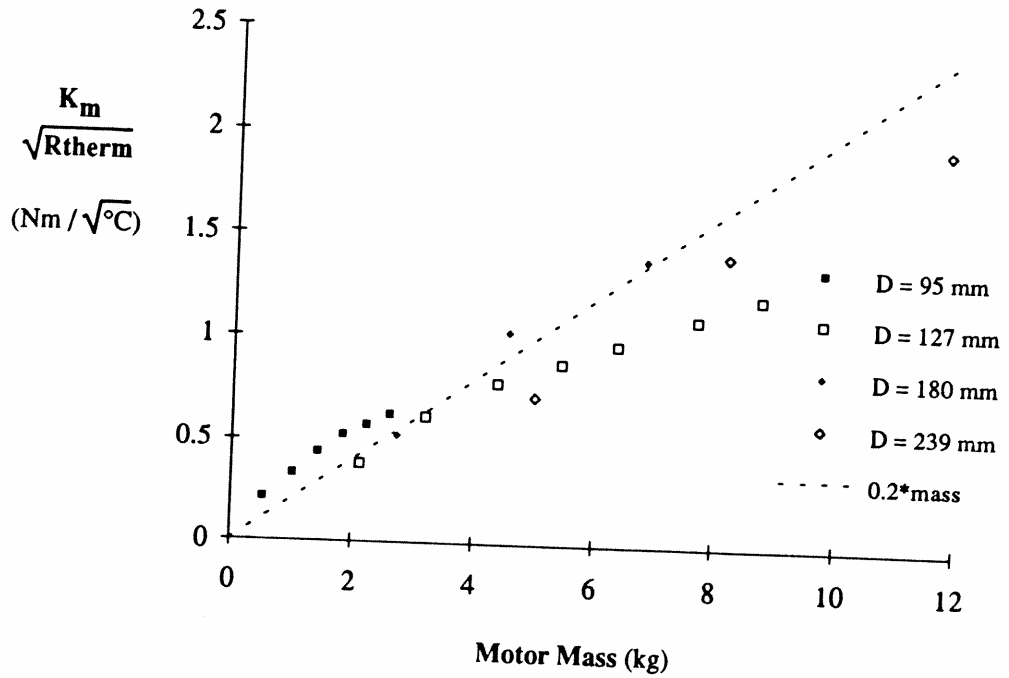

Figure 2: $K_m R_{therm}^{-1/2}$ *vs.* motor mass for Inland brushless motors.

A survey of motor specifications indicates that the mass/volume for housed motors ranges from 3000–5000 kg/m^3. (Note that the density of steel is 8000 kg/m^3.) Assume mass/volume = 3000 kg/m^3. For rare-earth designs, typically $2r = 0.7D$ (Ohno and Sugimoto, 1991), and the motor volume is $v = \pi(D/2)^2 l = 2\pi r^2 l$. The motor mass is $m = \rho v$, where ρ is the mass/volume, and hence the achievable torque/mass is

$$\tau_{cont}/m = i_l B_g/\rho \leq 6\,\text{N·m/kg} \tag{9}$$

using $\rho = 3000$ kg/m^3. A torque/mass of 6 N·m/kg is a relatively low value, evidently not subject to much improvement. On the other hand, relatively high power/mass can be achieved with EM motors by letting the motors spin fast. From Equation (5), the maximum mechanical power is delivered at $\omega_0 = \omega_{max}/2 = V/2K_T$. Mechanical power can be increased at the expense of torque by choosing a lower K_T; for example, in Table 1 the Aerotech model 1410-01 has the lowest K_T of 0.2 N·m/A. In addition, the mechanical power is limited by the volt-amp rating of the power electronics. For a given i_{cont} limited by thermal considerations, V could in principle be increased to any level of mechanical power desired. In practice, componentry in the power electronics limits the volt-amp rating. Thus for a given τ_{cont}, the continuous P_{mech} (and hence the speed ω_0) is somewhat arbitrary as it depends on the power electronics.

Power/mass therefore may not be a very good indicator for the intrinsic limits of EM motors, although it is an indicator of the total system limit (motor plus accompanying amplifier). For example, the Aerotech DS8020 servo amplifier has a rated continuous power output of 765 W and a maximum continuous current of $i_{cont} = 10$ A. The Aerotech 1410-01 motor would have an intrinsic current limit of $i_{cont} = \tau_{cont}/K_T = 2.89/0.2 = 14.5$ A, which is not achievable by the amplifier. The volt-amp curves for the motor indicate that 73 V and hence 730 W can be delivered continuously at 10 A. Hence the continuous mechanical power is $P_{mech} = P_{in} - P_{loss} = 730 - 112 = 618$ W. By contrast, the model 1410-02 motor which has the highest torque capability can be shown to produce the lowest power—318 W.

The total framed motor weight for the Aerotech model 1410-01 motor is 6 kg, and although the continuous torque/mass is low (0.5 N·m/kg) the continuous power/mass is reasonably good (100 W/kg). Yet the desirable operating speed of $\omega_0 = V/2K_T = 73/0.4 = 182.5$ rad/s (1,743 rpm) requires a gear reducer at a robot joint to be usable. From virtual work arguments, it can be shown that a gear ratio of α amplifies the motor torque to be $\alpha\tau$. From these various arguments, it is clear why the vast majority of commercial electric robots use dc motors with gears and why this situation is unlikely to change soon. As examples, the shoulder pitch drive has a gear ratio of about 50:1 for the PUMA 560 robot, 200:1 for the Cincinnati-Milacron T3 robot, and 1800:1 for the Spar SSRMS (space station remote manipulator system).

2.2.2 Direct Drive Motors

From a robotics standpoint, gearing results in the undesirable characteristics of friction, backlash, and flexibility (compliance), which make accurate control difficult. Recent interest has centered on the development of direct drive robots where high performance EM rotary motors actuate joints directly without intervening gears. A parallel is found in modern NC (numerically controlled) lathes where direct drive spindle motors have been recently introduced by a number of manufacturers (*e.g.*, Mazak). To achieve higher torques without using gears, these motors have to be made large. As indicated in Figure 2, high torque comes at the expense of high motor mass. For the Inland motors shown, which are typical of permanent magnet motors, $K_m/\sqrt{R_{therm}}$ per unit mass is about 0.2 N·m/$\sqrt{°C}$. Assuming an allowable temperature rise of 150 °C above ambient, a torque/mass ratio of about 2.5 N·m/kg is calculated. Note this is somewhat lower than the 6 N·m/kg limit calculated in Equation (9).

Improvements in torque/mass through design could focus on increasing K_m and reducing R_{therm}. For example, a group of us at McGill (Hollerbach and Hunter) and MIT (Lang, Umans, Garabieta, and Vaaler) have recently developed water-cooled synchronous motor prototypes (wound-rotor in pancake geometry); advantage is taken of the key feature of direct drive that rotor rotations are limited (less than 360°), and so water-cooling lines can easily be passed through joints. The water-cooling effectively reduces R_{therm}, and the result is a motor with a torque/mass of 15 N·m/kg. This torque will be realized at 2.5 rps, and hence the power/mass will be roughly 200 W/kg.

Progress in brushless motor drives (Leonhard, 1988) has been an enabling technology for direct-drive robotics. Because of problems caused by brushes, such as arcing at high currents and voltages, dc motors are not as suitable. The first direct drive robot employed Alnico dc torque motors (Asada, Kanade, and Takeyama, 1981), but in subsequent designs ac motors were used to circumvent problems with brushes (Asada and Youcef-Toumi, 1985). Two main kinds of ac motors have been selected for such robots: (1) synchronous motors with rare-earth permanent magnet rotors, and (2) switched reluctance drives.

Examples of commercial synchronous motors with rare-earth permanent magnet rotors include the ISI motors employed by Asada and Youcef-Toumi (1987).

Reluctance motors, unlike dc, induction, and synchronous motors, produce flux on one, not both, sides of the airgap. It was long assumed that reluctance motors were inferior at producing torque and tended to be used for clock motors and other very low power applications (Laithwaite,1975). In recent years work by Lawrenson and others (Lawrenson, 1980) has shown that high performance in reluctance motors is possible, though their theory of operation involves highly nonlinear magnetic behaviour, and their control involves relatively complicated and precise switching. Substantial torque ripple has typically been a problem, but recent advances in microprocessor control have reduced the torque ripple (Ilic-Spong *et al.*, 1987; Taylor, 1991).

Commercially, the Motornetics Megatorque motors, manufactured by NSK, have torque/mass up to 6.1 N·m/kg. The Superior Electric Company produces the SLO-SYN Direct Drive Servo Positioning System series, which have torque/mass of about 4 N·m/kg. Yokogawa Electric produce a series of hybrid motors called Dynaserv, which are variable reluctance but have windings which are biased with permanent magnets; the torque/mass ratio varies from 1.5 to 4.5 N·m/kg. Kuwahara *et al.* (1986) have developed a hybrid motor with an outside rotor that claims a torque/mass of 8.3 N·m/kg (frameless). These motors appear to achieve

torque/mass near or even higher than the 6 N·m/kg limit calculated earlier. This may be due in part to higher flux densities (since the machines are deliberately designed to have saturating magnetics) and to a large diameter, small length geometry, which tends to increase the surface area per mass, leading to a low R_{therm}.

Despite progress in ac motors, the torque/mass is still too low for general-purpose direct drive robots. Just gravity alone is too much of a load for these motors, and as a consequence present direct-drive robots require special configurations. One common approach is the SCARA configuration, where the first 3 rotary joints are horizontal and do not bear a gravity load (Kanade and Schmitz, 1985). The Adept-One robot (Curran and Mayer, 1985) has a SCARA configuration, but is not truly direct drive because of the use of belts. Another approach employs a 4–6 bar linkage transmission element for the elbow, and hence is not truly direct drive (Asada and Youcef-Toumi, 1987; Kazerooni and Kim, 1988). A third approach involves counterbalancing (An, Atkeson, and Hollerbach, 1988; Suehiro and Takase, 1985), but increased inertia and lower bandwidth result.

Another trend is to use low gear ratios with direct drive motors, to trade off nonlinear gear dynamics against improved torque (Takase, 1984; Vischer and Khatib, 1990; Youcef-Toumi and Nagano, 1987). For dc motors with geared drives, a trend is to improve the modeling of the gear dynamics to achieve more accurate joint torque control (Armstrong, 1990).

3 Hydraulic Actuators

Hydraulic actuators convert energy supplied by pressurized hydraulic fluid into rotary or linear motion. The earliest recorded contributor to fluid power is Ktesbios, an Alexandrian who lived from 285–247 B.C. (Maskrey and Thayer, 1978). In recent years, the marriage of electronics and hydraulics into electrohydraulic servomechanisms and demanding applications such as aerospace have led to increasing sophistication. Hydraulic fluid pumps are usually actuated with electromagnetic motors or internal combustion engines. The hydraulic fluid flowing through the hydraulic actuator is controlled either by servovalves which are usually electromagnetically actuated, or directly by variable-displacement pumps.

The output characteristics for ideal (lossless) linear and single-vane rotary hydraulic actuators are given in Table 2, where

Output	Linear Actuator	Rotary Actuator
Speed	$v = Q_c/A_c$	$\omega = Q_c/D_m$
Force or torque	$F = A_c p_l$	$\tau = D_m p_l$
Mechanical power	$P_{mech} = Q_c p_l$	$P_{mech} = Q_c p_l$

Table 2: Output characteristics of hydraulic actuators (Nakanishi, 1991).

Q_c is the control flow—the flow through the valve control ports to the load actuator.

p_l is the load pressure drop—the differential pressure between the control ports on the load actuator.

A_c is the pressure receiving area.

D_m is the volumetric displacement per radian of rotation.

A double-vane rotary actuator would double the torque produced, but halve the angular excursion.

Major types of servovalves are: sliding spool valves, flapper-nozzles, poppet or cartridge valves, and jet pipes (Blackburn *et al.*, 1960). A common combination is a two-stage valve incorporating a spool as the main valve and a flapper-nozzle as the pilot valve. A pilot valve is required to overcome large friction and restoring forces on the spool, whereas comparatively much less force is required to move the pilot. The flapper is rotated by a torque motor between two nozzles to regulate the spool motion.

Poppet or cartridge valves typically involve a seating action of a cone-shaped poppet into a cone-shaped orifice, under solenoid control. Advantages of four-poppet directional valves over sliding-spool valves include less pressure drop in the valve and hence greater efficiency, virtually no leakage, less hydrodynamic shock, and independent control of flow paths (Roberts, 1988). Disadvantages include highly nonlinear flow *vs.* displacement at small openings, larger time lag and hence slower speeds, and large and unpredictable operating forces (Blackburn *et al.*, 1960).

A jet pipe directs flow between two channels, typically through rigid rotation by a torque motor (Holzbock, 1986). Jacobsen and colleagues at the University of Utah (McLain *et al.*, 1989) have designed a single-stage, four-way, suspension valve that bends under control of an electromagnet (Figure 3).

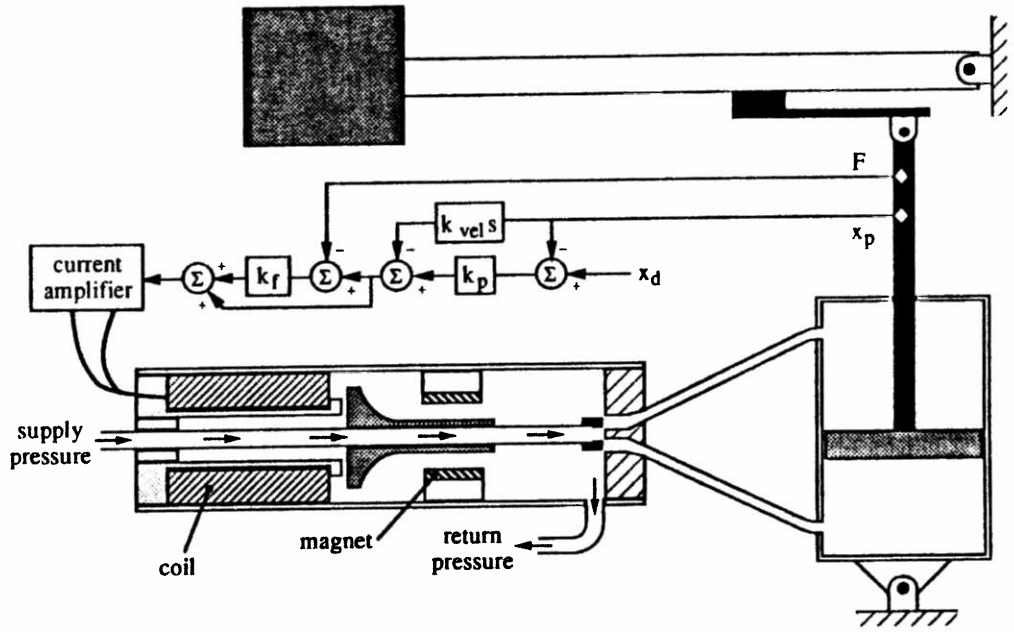

Figure 3: Single-stage, four-way, suspension valve controlling a double-acting hydraulic cylinder (McLain *et al.*, 1989).

3.1 Characteristics

The operating characteristics of a commercial hydraulic actuator depend on its technical specifications, provided by the manufacturer, and on the supply pressure p_s. The technical specifications for a rotary actuator include the displacement D_m and the rated flow Q_r, which is defined as follows (Thayer, 1962).

$p_v = (p_s - p_r) - p_l$: Valve pressure drop—the differential pressure drop across the control orifices of the servovalve. Assuming that the return pressure p_r is at atmospheric and the supply pressure is high yields $p_s - p_r \approx p_s$.

Q_{nl} : No-load flow—the control flow when $p_l = 0$. The load is moving freely and no torque is generated. This would correspond to the maximum rotational speed ω_{max} on the torque-speed curves for a dc motor.

Q_r : Rated flow—the no-load flow at full valve flow when $p_v = 6.7$ MPa (1000 psi). Call this pressure p_{vr}.

The no-load flow can be found from the rated flow for different supply pressures as follows (Clark, 1969):

$$Q_{nl} = Q_r \sqrt{p_s / p_{vr}}. \tag{10}$$

Flow (m^3/s)	**Speed** (rad/s)	**Torque** (kN·m)	**Power** (kW)
$Q_{nl} = 14 \times 10^{-4}$	$\omega_{max} = 2.2$	$\tau = 0.0$	$P_{mech} = 0.0$
$Q_c = 8.2 \times 10^{-4}$	$\omega = 1.3$	$\tau = 6.6$	$P_{mech} = 8.2$

Table 3: Performance of Hyd-ro-ac rotary actuator in the shoulder joint of the T^{3}586 robot.

At full valve opening, the control flow is related to the no-load flow by:

$$Q_c = Q_{nl}\sqrt{p_v/p_s}. \tag{11}$$

The mechanical power can be found from Table 2 and (10)–(11):

$$P_{mech} = Q_r(p_s - p_v)\sqrt{p_v/p_r}. \tag{12}$$

At $p_v = p_s/3$ the mechanical power is at a maximum, *i.e.*,

$$(P_{mech})_{max} = Q_r(2p_s/3)\sqrt{p_s/3p_r} \tag{13}$$

As an example (Holzbock, 1986), the shoulder axis for the Cincinnati T^{3}586 robot is driven by a double-vane Hyd-ro-ac rotary actuator produced by Bird-Johnson Co., whose angular range is 90°, rated flow Q_r is 9.5×10^{-4} m^3/s, and displacement D_m is 6.6×10^{-4} m^3/rad. The supply pressure is p_s = 15 MPa (2250 psi). Table 3 summarizes the no-load flow results and the control flow results for maximum power.

As a second example, we have used a Moog 730-233 servovalve with a Rotac 26R-5 two-vane rotary hydraulic actuator (Ex-Cell-O Corp., Greenville, Ohio) for testing of human ankle dynamics (Kearney *et al.*, 1983). At a supply pressure of 20 MPa (3000 psi), a torque of 2,790 N·m is produced; the actuator weighs 28.9 kg, which gives a torque/mass of 96 N·m/kg. The rated flow of the servovalve is $Q_r = 6.3 \times 10^{-4}$ m^3/s at p_{vr} = 6.7 MPa (1000 psi) valve pressure drop. The maximum power P_{mech} = 8.4 kW; hence the power/mass is 290 W/kg.

Such large torque/mass and power/mass are impressive in comparison to electromagnetic actuators, and explain their popularity for large robots and machinery. These ratios could be increased by increasing the supply pressure, but such problems as leakage, coupling, and routing would become more severe. The power/mass could also be increased by using a servovalve with a higher rated flow, although frequency response might suffer.

Electrohydraulic servovalves exhibit complex high-order, nonlinear dynamics, such as hysteresis of the electromagnetic valve element, variation of the orifice fluid-impedance with flow and fluid characteristics, change in orifice discharge coefficient with pressure ratio, and sliding friction for spools. The nonlinear dynamics of the two-stage flapper-nozzle with spool valve have been extensively studied (*e.g.*, Lin and Akers, 1991). At lower frequencies, low-order transfer functions can usefully represent the valve dynamics (Thayer, 1965). For their suspension valve, McLain *et al.*(1989) have found that 13 first-order nonlinear differential equations represent the dynamics well. Boulet *et al.*(1992) have also provided an experimentally tested nonlinear model for this suspension valve.

The frequency response of electrohydraulic servovalves depends on the number of stages: single-stage valves are the fastest, followed by two-stage valves, while hydrostatic actuators are the slowest (Maskrey and Thayer, 1978). Hydrostatic actuators involve direct control of a hydraulic actuator by a variable-displacement pump. More suited for large machinery, hydrostatic actuators are used in the OSU Active Suspension Vehicle (Pugh *et al.*, 1990), but recently their use has been proposed for robot arms (Bobrow and Desai, 1990). An advantage of the suspension valve over the spool valve is that the moving mass is much less and there is no friction, and hence higher servo rates are possible. In comparison to pneumatic actuators, hydraulic actuators are faster because the fluid is relatively incompressible.

3.2 Robotics Applications

There have been many applications of hydraulic actuators to robotics. Yet an overall trend of replacing hydraulic robots by electric robots has emerged, due to concerns about hydraulic supplies and leakage, improvements in geared electric drives, and complex control dynamics and lack of backdrivability for force control. Nevertheless, for high forces or torques and speeds hydraulic servoactuators outperform current electromagnetic actuators (Korane, 1990). With proper design, leakage can be virtually eliminated.

A series of new linear and rotary hydraulic actuators have been developed by Jacobsen and colleagues at the University of Utah, which have impressive torque/mass characteristics, high bandwidth, and even intrinsic compliance. The new Sarcos Dextrous Arm (Jacobsen *et al.*, 1991) is a 7 DOF (degree of freedom) redundant manipulator actuated by rotary hydraulic actuators at a pressure of 20 MPa (3000 psi). The torque/mass for the wrist, elbow, and shoulder actuators averages to

about 120 N·m/kg, and the power/mass to 600 W/kg. A caveat for the torque/mass ratio is that torque is a highly nonlinear function of mass, since larger actuators can have much higher ratios: the elbow actuator for the Sarcos Dextrous Arm was increased from 50 to 100 N·m by increasing the diameter by only 2 mm while keeping the length the same. Certain material overhead is required to have an actuator at all, such as bolts, passages, and output shafts, dictated primarily by geometry rather than by structural integrity. Innovative features include load cells at the joints, a drain system that uses a redundant set of seals and extra passageways to evacuate any fluid that might get by the high pressure seals, and the amalgamation of fluid routing with the actuator body to save on bearings, seals, weight, and space while providing a totally hard enclosure for the oil as it flows up and down the arm.

Wells *et al.*(1990) have considered other innovations for hydraulic actuators, including the use of accumulators to introduce more passive compliance, and the independent control of valve area on both the supply pressure side and the return pressure side. With such innovations, the revival of hydraulic actuator technology for robotics is promising.

4 Pneumatic Actuators

Pneumatic actuators and valves share many of the features of their hydraulic counterparts, but specific design and operating differences result from (i) the lower viscosity of air relative to hydraulic fluid (by a factor of 1000), (ii) the higher compressibility of air (by a factor of 300), and (iii) the poor lubrication of air relative to hydraulic fluid (Blackburn *et al.*, 1960). Practical consequences are (i) tighter tolerances to minimize leakage, and (ii) fast-acting valves to counteract gas compressibility.

Commonly, pneumatic actuators involve a piston driven by pressurized gas, much in the same way as in hydraulic actuators. For such actuators, Jacobsen *et al.* (1984, 1985) designed a two-stage valve comprised of a suspension-type jet pipe followed by a deflection jet pipe system positioned by antagonistic diaphragms. The commercial version embedded in the Utah/MIT Dexterous Hand uses a single-stage suspension valve, similar to the hydraulic servovalve reported in (McLain *et al.*, 1991).

Instead of pistons, inflatable elastic tubes or bladders surrounded by a braided mesh that shorten (contract) with pressure have become popular again. These actuators were extensively utilized in artificial limb research in the 1950s and 1960s (Hannaford and Winters, 1991),

under the name McKibben muscles. A similar actuator to the McKibben muscles is currently produced by Bridgestone, called the Rubbertuator (see Inoue, 1988), and consists of a rubber tube covered with a helical fiber braid. Immega (1987) has designed the ROMAC actuator, which consists of an articulating polylobe bladder and a steel cable harness.

Other esoteric pneumatic actuators involve applying forces using the mass flow of air jets. We have designed such a perturbation device for studying human arm dynamics, where the servovalve employs the Coanda effect to achieve high-frequency switching (Xu *et al.*, 1991).

4.1 Characteristics

The typical maximum supply pressure for pneumatic actuators is about $p_s = 670$ kPa (100 psi). For piston-type pneumatic actuators the thrust force f is given by (Saito, 1991):

$$f = \mu p_s A, \tag{14}$$

where A is the cross-sectional area of the cylinder, and μ is the thrust coefficient. The thrust coefficient depends on friction and air pressure; it approaches 1 at higher pressures, and so the force per area is the same as the supply pressure.

The braided pneumatic actuators produce a higher force per cross-sectional area at the same pressure. The static force versus pressure relationship for the McKibben muscle is (Hannaford and Winters, 1991):

$$f = p_s A_d (3\cos^2\theta - 1), \tag{15}$$

where θ is the angle between the elemental length of the helical fiber and the longitudinal axis of the tubing, and A_d is the cross-sectional area when the bladder is fully expanded. Thus the maximum force is about 3 times greater than for a cylinder with a piston. The actuator stiffness increases approximately linearly with pressure. For the Rubbertuator, the force-pressure characteristic is:

$$f = p_s A_0 \left[a(1-\epsilon)^2 - b\right], \tag{16}$$

where A_0 is the cross-sectional area before displacement, ϵ is the contraction ratio, and a and b are constants for the actuator. The Rubbertuator shortens by up to 20% ($\epsilon = 0.2$). Rubbertuators come in several sizes; the smallest (Rubbertuator #5) is 150 mm long, weighs 28 g, and generates a force of 800 N at a pressure of 600 kPa. Rubbertuator #5 has a resting cross-section of 0.5×10^{-4} m^2, and a maximal cross-section when

fully pressurized and shortened of 3.0×10^{-4} m^2 (Hannaford and Winters, 1991). Using the latter value, the force per area is 4 MPa. Without including the mass of the pneumatic servovalve, the peak force/mass is 28 kN/kg. Using quick-release tests, Hannaford and Winters (1991) estimate the peak power/mass as 10 kW/kg.

The ROMAC actuator, which contracts by up to 50% when inflated, can generate maximum tensions of over 300 kN/m^2 and peak force/mass ratios exceeding 50 kN/kg. These are impressive figures in comparison even to hydraulics. For comparison, muscle produces 350 kN/m^2 and, when the diameter is the same as its length, a maximum force/mass of 275 N/kg.

For pneumatic cylinders, to overcome limitations of compressibility on bandwidth, pressure control is considerably superior to flow control. Using active pressure sensing, Mannetje (1981) has shown that a 30 Hz bandwidth was achieved under pressure control for a spool valve design, but only 1.25 Hz was achieved under flow control. The two-stage servovalve design by Jacobsen *et al.* (1984,1985) acts mechanically as a pressure source because of the antagonistic diaphragms; they report a force bandwidth between 21–35 Hz, depending on the piston position in the cylinder. Liu and Bobrow (1988) implemented pressure control using active pressure sensing and a two-stage flapper-spool valve.

Information on the dynamic performance of the Rubbertuators and ROMAC pneumatic actuators is rather scant. Inoue (1988) has published results which show a Rubbertuator rotating a joint under angular position servo-control through a 1 rad step with a settling time of a little over 1 s at a peak angular velocity exceeding 2.5 rad/s. The high volume of the ROMAC actuator would mean greater filling time and hence lower bandwidths (Hannaford and Winters, 1991). It is important to realize that some pneumatic servovalve must exist to regulate pressure and air flow into these braided pneumatic actuators, and that the servovalve will ultimately limit the dynamic performance.

4.2 Robotics Applications

The Utah/MIT Dexterous Hand (Jacobsen *et al.*, 1986) employs a single-stage suspension valve to a glass cylinder with graphite piston. The servovalve weighs 0.068 kg, and has a no-load flow of 2.6×10^{-4} m^3/s at 670 kPa (100 psi). The cylinder is 0.1 m long and has a bore diameter of 0.016 m. The total weight of a single cylinder plus servovalve is 0.132 kg; some degrees of freedom employ a double piston arrangement, with total weight of 0.168 kg. The single cylinder arrangement produces 90 N of force, while the double cylinder arrangement produces 135 N.

This four-fingered hand, produced commercially by Sarcos Inc. (Salt Lake City, Utah), is currently the highest performance device of its kind and incorporates 32 of the electro-pneumatic actuators to drive the hand 16 DOFs (degrees of freedom).

Liu and Bobrow (1988) and Bobrow and Jabbari (1991) have investigated control methods to produce higher performance pneumatic actuators for robot joints. Kawamura *et al.* (1989) implemented a PI-type hierarchical feedback controller, which also uses pressure feedback, for positioning. Lai *et al.* (1990) investigated pulse width modulation (on-off) control of poppet valves for a Schrader Bellows 5-DOF manipulator.

Two types of robots incorporating the Rubbertuator have been commercialized (Inoue, 1988). The first is a horizontal multi-joint robot called the RASC. The second is a suspended multi-joint robot arm called the SOFT ARM which weighs a little over 30 kg and comes in two versions having 4 and 5 DOFs and a lifting capability of 1 and 3 kg respectively. Suzumori *et al.* (1991) have developed fiber-reinforced rubber actuators with up to 3 DOFs, and constructed a 3-fingered gripper and a 7-DOF arm with these novel pneumatic actuators.

Pneumatic actuators have the advantage that they produce tensions approaching muscle, have high force/mass ratios and can be fast when the servo-valve is integral. They are also inherently compliant (because of gas compressibility) which may be a desirable characteristic for certain applications.

5 Shape Memory Alloy Actuators

The shape memory effect for certain alloys involves, after a mechanical deformation, a return to an undeformed state when heated. The shape memory effect is caused by a martensite to austenite phase transition, which occurs progressively over a band of temperatures. By far the most popular shape memory alloy is NiTi because of its favorable material properties, nontoxicity and reasonable cost. In the lower temperature martensite phase, the NiTi has low crystal symmetry and can be readily plastically deformed. Upon heating to above the phase transition temperature band, the NiTi transforms to a higher symmetry crystalline austenite phase, having the same distribution of atoms as before the plastic deformation (Funakubo, 1991).

The parent phase configuration of NiTi, which may be simply a straight wire or coil spring, is achieved by holding the NiTi firmly in the desired configuration while heating to about 500 °C (*i.e.*, the annealing

temperature) for some time (*e.g.*, 1 hour). The NiTi is then cooled to above the transition temperature band and will retain its new shape. When it is further cooled below its transition temperature band it may then be readily deformed. Heating to above the transition temperature band will cause it to recover its shape. Recently, Ikuta *et al.* (1991) have reported an intermediate third phase under low-temperature annealing.

5.1 Characteristics

The electrical resistivity of NiTi increases by more than 20% in the phase transition from austenite to martensite (note that over a wider temperature range the change in resistivity is a complicated non-monotonic function of temperature with hysteresis). However, within and near to the phase transition temperature band this change in resistivity can be effectively used to control NiTi actuators.

The contraction time of NiTi is governed by the amplitude of the current pulse passed through it (and hence the heating time). By using large current pulses this contraction time can be made very short. The rate limiting part of the NiTi contraction and expansion cycle is in the relatively long time required for NiTi to cool back to its original length. The cooling time is governed by the fact that in both heating and cooling the usual thermal capacity has to be considered as well as the latent heat involved in the phase change between the austenite and martensite state (Ikuta, 1990). Figure 4 shows the twitch response (contraction then relaxation) of a single 100 mm long, 0.8 mm diameter NiTi fiber.

It is clear from this figure that such fibers are slower than muscle fibers. To speed up response without burning the fibers, Kuribayashi (1991) has used temperature sensing to regulate the SMA activation. We have attempted to improve the total contraction plus relaxation time and have found that by exposing NiTi fibers to massive electromagnetic fields we can change their properties (Hunter *et al.*, 1991). The modified NiTi now will shorten and lengthen very rapidly as shown in Figure 4. The twitch response is now faster than fast skeletal muscle.

The attraction of NiTi is the huge force per wire cross-section, which exceeds 200 MN/m^2. The power/mass ratio of modified NiTi fibers can also be large, at 50 kW/kg. Figure 5(a) shows the relation between applied stress and the peak power to mass ratio generated by a 100 mm long 0.8 mm diameter modified NiTi fiber subjected to a 24 V, 10 ms pulse. Figure 5(b) shows the incremental stress generated by a similar but modified NiTi fiber plotted against the applied stress.

The efficiency with which NiTi converts thermal energy to mechanical energy has been considered by McCormick (1987) and varies between

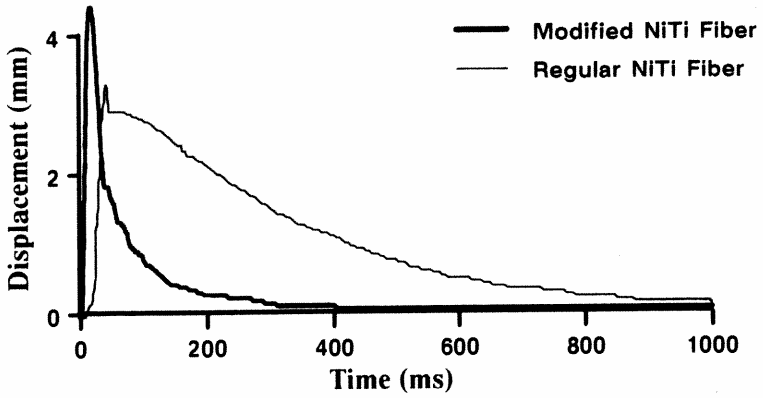

Figure 4: Displacement time function for NiTi for regular and modified fibers in response to a current pulse.

2–3% when there is full heat recovery of the heat associated with the thermal capacity. At present no method has been devised to recover this heat while retaining fast cycling. This is because current methods for producing relatively fast NiTi cycling involve continuous flow of a coolant over the NiTi.

5.2 Robotics Applications

A number of robot limbs have been constructed using NiTi fibers. For example, Hitachi has produced a robot hand using NiTi fibers (Nakano *et al.*, 1984). Kuribayashi (1986) reported on an antagonistic SMA-controlled joint. Ikuta *et al.* (1988) and Dario *et al.* (1991) have reported novel NiTi actuated worm-like endoscopes. Bergamasco et al. (1989) have reported experiments on an agonist-antagonist NiTi actuator for robotic applications. Homma *et al.* (1989) have built a small 5-DOF robot arm using NiTi fibers.

Many applications of NiTi use the fibers wound into the form of a coil spring. The maximum shear strain is usually limited to 1% to avoid fatigue. For applications requiring rotation (*e.g.*, robotic limbs) the two NiTi coil springs are often attached to a circular pulley to form an antagonistic pair. A problem with this design is that as the NiTi spring shortens, the force it generates varies, and hence so does the torque delivered by the joint. Recently, Hirose *et al.* (1989) have proposed a non-circular pulley whose shape was designed to enable the maximum generated torque to be held constant with rotation. Table 4 shows the basic characteristics of their NiTi actuator.

Ikuta (1990) has developed a small (30 × 40 × 14 mm, 27 g) gripper

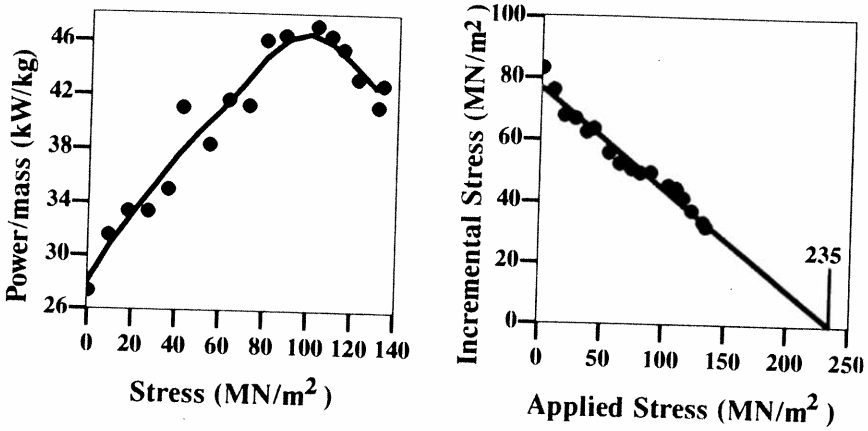

Figure 5: (a) Power/mass versus stress for NiTi. (b) Incremental stress versus applied stress.

having NiTi coil spring actuators (1 mm diameter coil, 0.2 mm diameter wire). The gripper response time is > 700 ms. An innovation in this work (see also Ikuta *et al.*, 1988) is the use of the change in resistance which accompanies the martensite to austenite transformation to directly control the NiTi. Kuribayashi and Yoshitake (1990) designed a thin-film bimorph SMA micro actuator, where the SMA is deposited onto a springy substrate that acts as an antagonist.

6 Polymeric Actuators (Contractile Polymers)

Various synthetic polymers are known to convert chemical or electrochemical energy into mechanical energy. They include polyelectrolyte gels, natural and synthetic rubber, and cross-linked collagen (see the review by Tatara, 1987). Gels can swell or shrink substantially and reversibly under small changes in external conditions such as pH, electric field, solvent condition, temperature, and even light (Irie, 1986).

The most promising contractile polymer in terms of strength, robustness, and response rate is currently a polyvinyl alcohol-polyacrylic acid (PVA-PAA) copolymer. Contraction/dilation is caused by three key forces: rubber elasticity, polymer-polymer affinity, and hydrogen ion pressure (Caldwell, 1990). Tatara (1987) estimates that the chemical to mechanical energy conversion efficiency of these gels can be as high as 30%.

PVA-PAA polyelectrolyte gels swell in dilute (*e.g.*, 0.05 M) NaCl

Range of Motion	±85 °
Angular velocity	0.28 rad/s
Maximum torque	1.1 N·m
Torque/mass	1.2 N·m/kg
Output power	6.32 W
Efficiency	5.7 %
Power/mass (NiTi)	216.4 W/kg
Power/mass (motor)	5.75 W/kg

Table 4: NiTi actuator developed by Hirose *et al.* (1989).

solution when a voltage is applied across them (see Chiarelli and De Rossi, 1988; De Rossi *et al.*, 1986; Chiarelli *et al.*, 1987). De Rossi *et al.* (1986) have proposed that the contraction is largely a result of pH gradients (established by the electrode reactions), which propagate through the gel by electrodiffusion. The resulting perturbations in the electrostatic interactions between polyelectrolyte ionized groups cause mechanical deformation of the gel. Acetone activation of PVA gels has been investigated by Caldwell and Taylor (1990) and Suzuki (1991).

6.1 Characteristics

Chiarelli *et al.* (1987) have reported that a 10 mm wide 0.11 mm thick strip of electrochemically activated PVA-PAA gel can generate an isometric force of up to 0.1 N. This corresponds to a force density of 91 kN/m^2. This is consistent with force densities as high as 125 kN/m^2 reported by De Rossi *et al.* (1986), who by extrapolation also predict that 1 mm thick gels should be able to reach force densities of 300 kN/m^2 and strain rates of 5 to 10 s^{-1}. At present the contractions are very slow; for example, the strip just mentioned in Chiarelli *et al.* (1987) took about 1000 s to contract to within 20% of its final maximum force.

Osada *et al.* (1989) and Kishi and Osada (1989) have reported work on the contractile behavior of similar polyelectrolyte gels and recently have reported work on these gels in the form of microparticles. The microparticles (150 to 300 μm diameter) shrank by 90% of their volume within 50 s. Kishi and Osada (1989) predict by extrapolation that 1 μm diameter microparticles should shrink by 95% of their volume in 0.23 ms. Currently there is insufficient knowledge about the physics of these microparticles, and further experimentation is required.

Caldwell (1990) reported that the force-velocity curve of artificial

PVA-PAA muscle fibers is similar to that of natural muscle. The maximum power/mass was 5.8 W/kg (referred to the dry mass of the polymer), much less than for muscle.

Suzuki (1991) examined methods for increasing the power density and response time of polymeric gel films. Response time increased as the square of film thickness; for a thin gel film 10 microns thick under acetone control, he achieved 100 kW/m^3 and a response time of 0.2 s.

6.2 Robotics Applications

Tatara (1987) has reported a piston packed with ion-exchange resin which contracts and expands when immersed in HCl and water respectively. Contraction and expansion (swelling) was rather slow but by using small diameter resin particles the expansion step response time was reduced to about 5 s. The force density of this piston was an impressive 2 MN/kg. Rather preliminary applications of contractile polymers to robots are presented in the review by Tatara (1987).

Caldwell (1990) designed a gripper system employing antagonistic polymeric actuators. Cycle times of 15 s and positional accuracy of 2° were achieved. Suzuki (1991) constructed an artificial elbow actuator from a bundle of hydrogel films 60 microns thick and 12 cm long, which could raise a 2 g load in 5 s.

Although the mechanisms of various contractile polymers are quite different from muscle, they are nevertheless more similar to muscle than any other actuator technology. So far they suffer from having serious fatigue problems and are too slow, but the speed of response, which is often limited by diffusion rate, should improve dramatically with miniaturization.

7 Piezoelectric Actuators

When forces are applied to certain crystals, they generate a charge which is roughly proportional to the applied mechanical stress (force). Conversely, an applied voltage generates deformation of the crystal. Cady (1964) has reviewed the early history of this area.

A simplified model of ceramics involves the notion of anions (−) and cations (+) connected by springs forming a crystal lattice (Uchino, 1986). Cations move in the direction of an applied electric field while the anions move in the opposite direction. The forces thereby generated cause lattice deformation. Piezoelectric materials have both high and low stiffness ionic bonds (*i.e.*, are noncentrosymmetric crystals) and

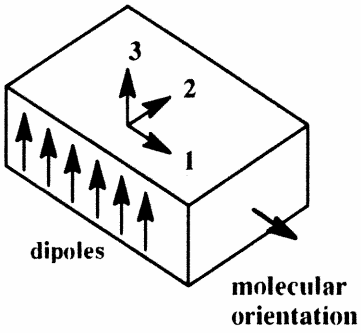

Figure 6: (a) Piezoelectric material terminology. (b) Piezoelectric hysteresis

have an induced strain vector **s** which is roughly proportional to the applied electric field vector **E**. The electromechanical coupling is direction dependent and so is specified by a material dependent piezoelectric tensor **d**; thus $\mathbf{s} = \mathbf{dE}$. Figure 6(a) shows the numbers assigned to each direction in a piezoelectric material. For example, for the tensor element d_{31} the subscript 3 defines the electric field direction and the subscript 1 the mechanical stress direction. s_1 is one of the resulting transverse strains and s_3 the longitudinal strain (in the direction of E).

Other phenomena complicate this simplified view. In particular, additional nonlinear strains resulting from crystalline domain reorientation cause the ubiquitous hysteresis seen in piezoelectric materials during changes in electric field (Figure 6(b)).

7.1 Characteristics

The material constants for one particular piezoelectric ceramic NEPEC-10 (Yano and Takahishi, 1989) are listed in Table 5. The maximum electric field is approximately $E_{max} = 10^6$ V/m, and a comparison of transverse and longitudinal piezoelectric effects is given in Table 6. For this material, the strain and electromechanical conversion efficiency is higher in the longitudinal direction than in the transverse direction. The stress is reported as 35 MPa in the longitudinal direction.

In terms of the imposed voltage V, for a slab 10 mm on a side a relatively high 10 kV would be required. To reduce the required voltage, Yano and Takahishi (1989) report on a piezoelectric stack with interleaved electrodes and piezoelectric plates that requires only 100 V for a slab of roughly this size.

Strains from piezoelectric materials are often too small to be directly useful, and various mechanisms have been created to amplify

Constant name	Symbol	Value	Unit
Piezoelectric constant	d_{31}	-287	10^{-12} m/N
	d_{33}	635	
Elastic modulus	c_1	67.6	10^9 N/m^2
	c_3	55.2	
Density	ρ	8.0	10^3 kg/m^3

Table 5: Material constants for piezoelectric ceramic NEPEC-10.

Constant name	Symbol	Value
Maximum strain	s_1	-0.3×10^{-3}
	s_3	0.6×10^{-3}
Electromechanical conversion efficiency	k_1	0.16
	k_3	0.46

Table 6: Comparison of transverse and longitudinal piezoelectric effects in NEPEC-10.

these strains. Polyvinylidene fluoride (PVDF), a common ferroelectric polymer, has been formed into a bimorph by electroding and bonding together two strips with opposing piezoelectric expansion axes. For a cantilever mounted piezoelectric bimorph, the unloaded deflection δ of the beam resulting from the applied voltage V is given by

$$\delta = \frac{3}{5} d_{31} V \left(\frac{L}{a}\right)^2 \tag{17}$$

where a is the width of each strip, L is the length, and $d_{31} = 2 \times 10^{-11}$ m/V for PVDF (Umetani and Suzuki, 1980). As an example, if $a =$ 0.5 mm, $L = 30$ mm, and $V = 300$ V, then $\delta = 13\,\mu$m.

A linear microstepping action can be obtained from a stick-slip mechanism. A platform makes frictional contact with the ground, and on the platform is a piezoelectric element and attached mass. Reaction forces that result from rapid acceleration of the mass by the piezoelectric element cause the platform to make a microstep. The mass is then retracted slowly enough so that friction prevents return motion of the platform. Niedermann *et al.* (1988) reported a small device for scanning microscopy which can move over arbitrary distances on a plane surface by moving in small (*e.g.*, 10 to 150 nm) steps. Matsuda and Kaneko (1991) report on a piezoelectric tube actuator for use in scanning tun-

neling microscopes. The tube actuator is a cylinder that bends in two directions and that moves a sample mounted on the end face of the cylinder by the stick-slip phenomenon.

Yano *et al.* (1989) report on a two-stage cantilever mechanism for a printer head. The amplification factor is 30, and strokes of 400 μm are achieved at 3,051 Hz with an impact force of 7.8 N.

Ultrasonic motors can be made from piezoelectrics, either of the vibratory coupler type or the surface wave type (Uchino, 1986). In terms of the vibratory coupler type, Burleigh Instruments (Fishers, NY 14453) produce commercially an inchworm piezoelectric motor used extensively for moving optical components. The surface wave type has recently become popular in camera focusing mechanisms. The energy transformation efficiency is relatively low.

Piezoelectric ceramics show substantial hysteresis, and hence piezoelectric actuators cannot be driven open-loop and accurate positioning is required.

7.2 Robotics Applications

Umetani and Suzuki (1989) employed PVDF bimorphs to create a microgripper and a 2-DOF microrobot arm. Tzou (1989) designed a two-jaw microgripper using PVDF bimorphs. Wang *et al.* (1990) designed a linear micropositioner from rectangular bimorphs of PZT-5. The use of piezoelectrics to control flexible-link manipulators has been investigated by Tzou *et al.* (1989) and Jiang *et al.* (1991).

Lee and Arjunan (1989) designed a 3-DOF micro-motion wrist, which utilizes a single cantilever to yield rotations of a movable platform of 0.02°. Hatamura and Morishita (1990) designed a 3-DOF linear microrobot that uses a mechanism of deformation of parallel plates. The full-stroke displacement for each axis is 12.5 μm and the accuracy is 0.01 μm.

Higuchi *et al.* (1990) applied the stick-slip stepping mechanism to design two types of microrobot joints. One was a single-DOF rotary joint, the other a 3-DOF ball joint.

We have designed a micro-motion robot that utilizes 3-axis parallel-drive manipulators, where each axis is a serial combination of a linear EM motor and a piezoelectric slab attached to quartz rods (Hunter *et al.*, 1990). The quartz rods from each axis meet at right angles at the tip, which contains a microgripper and force sensor. Motion occurs by beam bending, over a volumetric dynamic range for position from 1 nm to 1 mm. The bandwidth is 686 Hz for 100 μm amplitudes and 1047 Hz for 1 μm displacements.

8 Magnetostriction

Magnetostrictive materials change dimensions in the presence of a magnetic field. This effect had been thought to be a relatively small one, but over the last 30 years rare earth alloys have been developed that show very high maximum (magnetic saturation) magnetostrictive strains. An alloy containing both terbium and dysprosium, $Tb_{0.27}Dy_{0.73}Fe_{1.9}$, called Terfenol-D, has a strain of 0.002. These materials expand in a magnetic field.

The effect, known as *magnetostriction*, is caused by magnetic domains in the material aligning themselves with the direction of the magnetic field with a consequent change in material dimensions (see Clark, 1980). The magnetic field is usually generated by a coil wound around a rod of Terfenol-D. By changing the current in the coil the magnetic field is changed and hence the rod changes length.

8.1 Characteristics

Some of the properties of Terfenol-D are a function of the technique used to grow the material. Recently (see Clark *et al.*, 1989) techniques have been developed to produce highly grain oriented rods which result in maximal strains. Table 7 lists the basic properties of Terfenol-D. A particular problem is the low tensile strength (Peterson *et al.*, 1989), which usually means that actuator designs must provide some means to keep the Terfenol-D rod under permanant compression. The change in length of Terfenol-D as a function of magnetic field strength is shown in Figure 7. The large fields required to achieve 0.2% length changes typically require water-cooled coils.

As with piezoelectric actuators such as PZT, the maximum strain declines roughly linearly with increased force output (load). However, Terfenol-D has a very high energy density of 14 to 25 kJ/m^3 compared with 0.7 to 1.3 kJ/m^3 for PZT. Thus for high force applications, Terfenol-D would be preferable. In actual applications, magnetic fields of 0.5 T are employed, and forces of 2 MPa are produced (Goodfriend, 1991). Bandwidths can exceed 2000 Hz.

For displacements larger than 0.2%, "inch-worm" type linear stepping actuators (sometimes called *magnetoelastic wave motors*) have been developed (Kiesewetter, 1988). These motors, which move in small steps (*e.g.*, 10 μm), can move over substantial displacements (*e.g.*, 50%) at relatively low velocities (*e.g.*, 0.01 m/s).

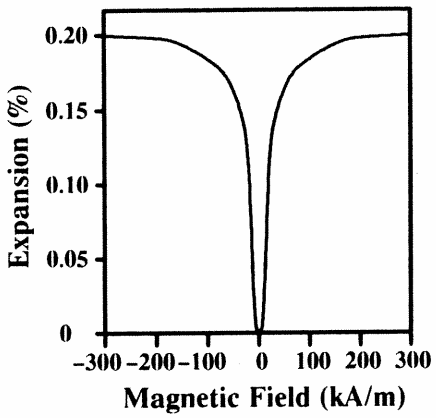

Figure 7: Expansion of Terfenol-D as a function of magnetic field strength.

Recently, hybrid Terfenol-D and PZT motors have been developed (see Akuta, 1989) in an attempt to extract the best qualities from both magnetostrictive and piezoelectric actuator technologies.

8.2 Robotics Applications

The use of magnetostrictive materials has largely been confined to the construction of actuators for underwater sound generation (*e.g.*, Butler and Ciosek, 1980). Magnetostrictive actuators have also been built for use in active attenuation of vibration (see Hiller *et al.*, 1989). The only robotics application we are aware of is the work of Fukuda *et al.* (1991), who built a mobile robot for pipe inspection. A magnetic field must be generated externally to the pipe, which is a drawback of this approach.

Long term prospects for magnetostrictive materials are promising because of the very high energy density, but various roadblocks for robotics applications exist. Like piezoelectrics, the strains are small and must be amplified. The wave motors mentioned above have not yet matured to a useful point; they are currently too slow. Large coils are required to generate the magnetic fields, and induction and heating limit the bandwidth. The material is brittle and hard to machine; its tensile strength is very low.

9 Muscle, Nature's Actuator

Skeletal muscle fiber (a single cell), the basic unit actuator for movement, is almost identical (same molecular machinery, similar diameters,

Basic Properties of Terfenol-D (from Edge Technologies, Iowa)		
Mass density	9.250	kg/m^3
Bulk modulus	90	GN/m^2
Young's modulus	25–35	GN/m^2
Tensile strength	28	MN/m^2
Compressive strength	700	MN/m^2
Thermal expansion	12×10^{-6}	/°K
Resistivity	0.6	$\mu\Omega$·m
Magnetostriction	$1.5–2.0 \times 10^{-6}$	
Energy density	14–25	kJ/m^3

Table 7: Properties of Terfenol-D.

same force per unit cross-section) across all mammals from the smallest mammal (20 mm long shrew) to the largest (blue whale). It is simply that an elephant or whale muscle has more muscle fibers in parallel than corresponding muscles in humans, mice and shrews. Thus nature has developed a modular actuator which is simply scaled up to produce more force by incorporating more muscle fibers in the muscle. Longer fibers are used where large displacements must be produced.

9.1 Characteristics

Muscle is activated by action potentials generated via nerves or directly by electrodes. For a single muscle fiber held at constant length, a single action potential or pulse generates a time-varying force termed a muscle twitch (Figure 8(a)). When muscle is stimulated by a series of pulses, the responses sum nonlinearly (labeled *unfused* in the figure). For a sufficiently high stimulation rate, the force rises smoothly and remains constant; this state is termed *fused tetanus*. Increasing the stimulation rate above this tetanic rate does not result in higher forces; thus we have a saturation nonlinearity.

When muscles contract against a load they shorten at a constant velocity (except for an initial transient and for large displacements). This constant velocity epoch is load-dependent in a characteristic manner expressed as the force-velocity relation; Figure 8(b) shows a typical force-velocity relation (Edman, 1979). The velocity in this plot is expressed as a strain rate because the velocity of any contracting fiber is proportional to its length. The maximum speed with which a limb can move

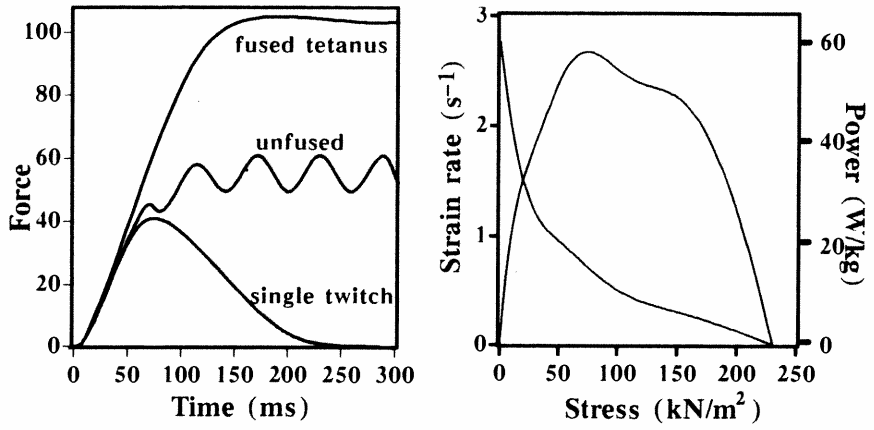

Figure 8: (a) Twitch, unfused, and fused tetanic responses. (b) Strain rate and power versus stress for a tetanized muscle.

is limited by the maximum shortening velocity of the muscles driving the limb. Muscles in different parts of the body have different maximum shortening velocities. Muscle training (*e.g.*, athletic activities) changes the maximum shortening velocity of muscles.

Although muscle mechanical properties are quite nonlinear, for a fixed activation and length these properties are well described as a second-order linear system. In particular, muscle stiffness is proportional to force (Hunter and Kearney, 1982).

The maximum force generated per unit cross-sectional area of vertebrate muscle fibers seems to be remarkably constant at about 350 kN/m^2 (Huxley, 1980).

Unlike maximal force, the maximum power (*force* $\times$ *velocity* or *stress* $\times$ *strain rate*) generated by muscle does vary both within the same organism as well as across animals. The maximum power is produced at about 1/3 of the maximum strain rate (which as it happens corresponds to a load of about 1/3 of the maximum stress the muscle can generate). Consequently the maximum power a muscle can generate is roughly 0.1 *maximum stress* $\times$ *maximum strain rate*. The maximum power per unit mass (in W/kg) is an important figure of merit for robotic actuators. For vertebrate muscle,

$$Power/mass \approx 35 \times strain\ rate$$

The maximum power/mass generated by the muscle fiber data plotted in Figure 8(b) is 53 W/kg. Human muscle is typically about 50 W/kg but can be as high as 200 W/kg for very brief periods.

9.2 Robotics Applications

As was mentioned earlier, muscle is used by nature almost exclusively for actuation from sub-millimeter organisms to the earth's giants, whales. Muscle cells can now be cultured and it is possible that in the future muscle could be grown for use in advanced robot designs.

10 Discussion

In this article, a number of actuator technologies relevant for robotics have been reviewed. We assemble here various actuator characteristics for comparison. First, Table 8 compares some material properties of the media which are the force sources for the different actuators. The stress for EM motors is derived from the tangential force per area in the airgap, while for hydraulic and pneumatic actuators it is the fluid pressures. The strains for the first 3 actuators are set roughly at 0.5 to reflect rough ranges of motion of cores of linear EM motors and of pistons in hydraulic or pneumatic linear motors.

The strain rate for linear EM motors was estimated for a 0.1 m long motor and a typical maximum velocity of 1 m/s. The strain rate for hydraulic actuators was estimated from the Sarcos Dexterous Arm rotary actuators. The pneumatic strain rate was estimated for the actuators for the Utah/MIT Dexterous Hand. The polymeric actuator characteristics reflect an extrapolation by De Rossi; current performance is much worse. The strain rates for piezoelectric and magnetostrictive materials are limited by the rate of electric or magnetic field application; the value for piezoelectrics represents a 0.4 ms voltage ramp to 230 V (Takahishi *et al.*, 1983) and for magnetostriction of reported bandwidths of 2000 Hz (Goodfriend, 1991). For single bursts of activation, it is possible to get much higher strain rates for these actuator materials.

In terms of traditional macro-motion actuator technology, the lowest stress by far is from electromagnetics, while pneumatics looks reasonably good in comparison to muscle and hydraulics is excellent. Of the newer macro-motion actuator technologies, polymeric actuators should have roughly the same stress as muscle and a good maximum strain of 50%. SMA has the best stress by far, but its efficiency is low. The strain for SMA can be up to 10%, but to avoid fatigue, strains of 1% are preferable. The micro-motion actuators—piezoelectrics and magnetostrictives—have very good stress characteristics, comparable to hydraulics. Their low strains, however, present difficulties for macro-robotic applications.

Actuator	**Stress** (MPa)	**Strain**	**S.R.** (s^{-1})	**M.E.**
Electromagnetic	0.02	0.5	10	0.9
Hydraulic	20	0.5	2	0.8
Pneumatic	0.7	0.5	10	0.9
NiTi SMA	200	0.1	3	0.03
Polymeric	0.3	0.5	5	0.3
Piezoelectric	35	0.001	2	0.5
Magnetostrictive	10	0.002	2	0.8
Muscle	0.35	0.2	2	0.3

Table 8: Material properties of actuator media. S.R. is the strain rate, M.E. is the mechanical efficiency.

These material properties have to be incorporated into complete actuators, which may realize each material's potential to varying degrees. Thus a housing and bearings are required for EM motors, servovalves for hydraulic and pneumatic actuators, cooling system for SMA, an activation system for polymerics, and motion scaling mechanisms for piezolectric and magnetostrictive actuators. In Table 9, selected actuators have been chosen to demonstrate the torque/mass and power/mass capabilities realized to date. In this table, in making an overall comparison of linear and rotary actuators, power/mass is relatively straightforward but force/mass *vs.* torque/mass is not. To do so, we have converted the force/mass of linear actuators to an equivalent torque/mass by selecting a lever arm as follows. A maximum of 60° rotation is to be produced at the full stroke of the linear actuator; this determines the insertion point. The choice of 60° means that peak torque is simply the product of peak force and maximum displacement.

Table 9 indicates that different degrees of success have been obtained in realizing the media properties of Table 8 as actuators. The first 3 traditional robot actuator technologies are more or less near the limits of the medium properties listed in Table 8. The (frameless) specifications for the McGill/MIT EM motor are well placed relative to the other listed actuator technologies. Nevertheless, hydraulic actuators continue to have the overall best characteristics; with design advances for bandwidth, intrinsic compliance, and better packaging championed by such groups as Jacobsen and colleagues, hydraulic actuators appear to be the actuation to beat for general macrorobotics.

The actuator characteristics for NiTi SMA and polymeric actuators

Actuator	**Torque/mass**	**Power/mass**
McGill/MIT EM Motor	15 N·m/kg	200 W/kg
Sarcos Dexterous Arm electro hydraulic rotary actuator	120 N·m/kg	600 W/kg
Utah/MIT Dexterous Hand electropneumatic servovalve	20 N·m/kg	200 W/kg
NiTi SMA (Hirose *et al.*, 1989)	1 N·m/kg	6 W/kg
PVA-PAA polymeric actuator (Caldwell, 1990)	17 N·m/kg	6 W/kg
Burleigh Instruments inchworm piezoelectric motor	3 N·m/kg	0.1 W/kg
Magnetoelastic (magnetostrictive) wave motor (Kiesewetter, 1988)	500 N·m/kg	5 W/kg
Human biceps muscle	20 N·m/kg	50 W/kg

Table 9: Comparison of actuator characteristics.

appear to fall far short of what should be possible, especially with regard to power/mass. Advances in activation methods for NiTi and for polymeric gels should yield more favorable characteristics in the future. The power/mass for piezoelectric and magnetostrictive actuators are low; this reflects the problem of scaling up their very small motions. The two-stage cantilever printhead mechanism of Yano *et al.* (1989) shows some promise in this regard. The scaling problems for magnetostrictive actuators are more severe, and their potential for general robotics doesn't appear too favorable at present.

According to Table 9, muscle has reasonable characteristics relative to other actuators, but these characteristics cannot be said to be outstanding. One issue that casts muscle in a better light is a compact and portable power source (the body). The issue of mobile power sources for robotics has not been dealt with here, but it is increasingly a concern for mobile robots and space robots.

This brief survey has necessarily sampled the domain of potential robot actuators. We have left out important and fast-developing areas such as magnetic bearings and levitation (*e.g.*, Hollis *et al.*, 1991), and micro electromechanical systems and electrostatic actuators (*e.g.*, Trimmer and Jebens, 1989). Potential developments such as combustion actuators and superconducting EM motors have also not been considered. Nevertheless, this survey has indicated the considerable progress

in robot actuators in recent years, and hopefully has given some idea of what might be expected in the future.

Acknowledgement

This work was supported by the US Office of Naval Research under grants N00014-89-J-1745 and N00014-90-J-1849. We thank Paolo Dario, Barry Hanover, Fraser Smith, and Erik Vaaler for their valuable comments.

References

[1] Akuta, T. An application of giant magnetostrictive material to high power actuators. *10th Intl. Workshop on Rare Earth Magnets and their Applications,* 1989, pp. 359–368.

[2] An, C.H., Atkeson, C.G. and Hollerbach, J.M. *Model-Based Control of a Robot Manipulator.* MIT Press, Cambridge, Massachusetts, 1988.

[3] Armstrong, B. Control of machines with non-linear low-velocity friction. *Experimental Robotics 1 — The First International Symposium,* edited by V. Hayward and O. Khatib, Springer-Verlag, New York, 1990, pp. 180–195.

[4] Asada, H., Kanade, T., and Takeyama, I. Control of a direct-drive arm. *J. Dynamic Systems, Meas., Control, 105,* 1983, pp. 136–142.

[5] Asada, H., and Youcef-Toumi, K. *Direct-Drive Robots: Theory and Practice.* MIT press, Cambridge, Massachusetts, 1987.

[6] Bergamasco, M., Salsedo, F., and Dario, P. A linear SMA motor as direct-drive robotic actuator. *Proc. IEEE Intl. Conf. Robotics and Automation,* May 1989, Scottsdale, Arizona, pp. 618–623.

[7] Blackburn, J.F., Reethof, G., and Shearer, J.L. *Fluid Power Control,* Technology Press of MIT, Cambridge, Massachusetts, 1960.

[8] Bobrow, J., and Desai, J. Modeling and analysis of a high-torque, hydrostatic actuator for robotic applications. *Experimental Robotics 1—The First International Symposium,* edited by V. Hayward and O. Khatib, Springer-Verlag, New York, 1990, pp. 215–228.

[9] Bobrow, J.E., and Jabbari, F. Adaptive pneumatic force actuation and position control. *J. Dynamic Systems, Meas., Control, 113,* 1991, pp. 267–272.

[10] Boulet, B., Daneshmend, L., Hayward, V., and Nemri, C. System identification and modelling of a high performance hydraulic actuator. *Experimental Robotics II,* edited by R. Chatila and G. Hirzinger, Springer-Verlag, 1992.

[11] Butler, J.L., and Ciosek, S.L. Rare earth iron octagonal transducer. *J. Acoustical Society of America, 67,* 1980, pp. 1809–1811.

[12] Cady, W.G. *Piezoelectricity.* McGraw-Hill, New York, 1946. Revised edition by Dover Publications, New York, 1964.

[13] Caldwell, D.G. Pseudomuscular actuator for use in dexterous manipulation. *Med. and Biol. Engrg. and Computing, 28,* 1990, pp. 595–600.

[14] Chiarelli, P., Genuini, G., and De Rossi, D. Electrochemically driven muscle-like actuators. *Proc. IEEE Conf. Engineering in Medicine and Biology,* 1987, pp. 1089–1091.

[15] Chiarelli, P., and De Rossi, D. Determination of mechanical parameters related to the kinetics of swelling in an electrically activated contractile gel. *Progress in Colloid and Polymer Science, 78,* 1988, pp. 4–8.

[16] Clark, A.E. Magnetostrictive rare earth-Fe2 compounds. In *Ferromagnetic Materials, 1,* edited by E.P. Wohlfarth, North-Holland, 1980, pp. 531–589.

[17] Clark, A.E., Teter, J.P., Wun-Fogel, M., Moffett, M., and Lindberg, J. Magnetomechanical coupling in Bridgman grown Tb0.3Dy0.7Fe1.9 at high drive levels. *34th Conference on Magnetism and Magnetic Materials,* Boston, 1989, pp. 1–12.

[18] Clark, D.C. *Selection and Performance Criteria for Electrohydraulic Servodrives.* Technical Bulletin 122, Moog Inc., East Aurora, New York 14052, 1969.

[19] Curran, R., and Mayer, G. The architecture of the AdeptOne direct-drive robot. *Proc. American Control Conf.,* Boston, June 19–21, 1985, pp. 716–721.

[20] Dario, P., Valleggi, R., Pardini, M., and Sabatini, A. A miniature device for medical intracavitary intervention. *Proc. IEEE Workshop on Micro Electro Mechanical Systems,* Nara, Japan, January 30–February 2, 1991, pp. 171–175.

[21] De Rossi, D., Chiarelli, P., Buzzigoli, G., Domenici, C. and Lazzeri, L. Contractile behavior of electrically activated mechanochemical polymer actuators. *Trans. American Society for Artificial Internal Organs, 32,* 1986, pp. 157–162.

[22] Edman. The velocity of unloaded shortening and its relation to sarcomere length and isometric force in vertebrate muscle fibres. *J. Physiol., 291,* 1979, pp. 143–159.

[23] Goodfriend, M. Material breakthrough spurs actuator design. *Machine Design,* March 21, 1991, pp. 147–150.

[24] Fukuda, T., Hosokai, H., Ohyama, H., Hashimoto, H., and Arai, F. Giant magnetostrictive alloy (GMA) applications to micro mobile robot as a micro actuator without power supply cables. *Proc. IEEE Workshop on Micro Electro Mechanical Systems,* Nara, Japan, January 30–February 2, 1991, pp. 210–215.

[25] Funakubo, H. *Shape Memory Alloys,* Gordon and Breach Science Publ., New York, 1991.

[26] Hannaford, B., and Winters, J. Actuator properties and movement control: biological and technological models. *Multiple Muscle Systems: Biomechanics and Movement Organization,* J.M. Winters and S. L-Y. Woo, eds., Springer-Verlag, New York, 1990, pp. 101–120.

[27] Hatamura, Y., and Morishita, H. Direct coupling system between nanometer world and human world. *Proc. IEEE Workshop on Micro Electro Mechanical Systems,* Napa Valley, California, February 11–14, 1990, pp. 203–208.

[28] Higuchi, T., Yamagata, Y., Kudoh, K., and Iwasaki, K. Micro robot arm utilizing rapid deformations of piezoelectric elements. *Robotics Research: the Fifth International Symposium,* H. Miura and S. Arimoto, eds., MIT Press, Cambridge, Massachusetts, 1990, pp. 37–46.

[29] Hiller, M.W., Bryant, M.D., and Umegaki, J. Attenuation and transformation of vibration through active control of magnetostrictive Terfenol. *J. Sound and Vibration, 133,* 1989, pp. 1–13.

[30] Hirose, S., Ikuta, K., and Umetani, Y. Development of shape-memory alloy actuators. Performance assessment and introduction of a new composing approach. *Advanced Robotics, 3,* 1989, pp. 3–16.

[31] Hirose, S., Ikuta, K., and Sato, K. Development of a shape memory alloy actuator. Improvement of output performance by the introduction of a s-mechanism. *Advanced Robotics, 3,* 1989, pp. 89–108.

[32] Hollis, R.L., Salcudean, S., and Allan, A.P. A six degree-of-freedom magnetically levitated varible compliance fine-motion wrist: design, modeling, and control. *IEEE Trans. Robotics and Automation, 7,* 1991, pp. 320–332.

[33] Holzbock, W.G. *Robotic Technology: Principles and Practice.* Van Nostrand Reinhold Co., New York, 1986.

[34] Homma, D., Miwa, Y., and Iguchi, N. Micro robots and micro mechanisms using shape memory alloy. *3rd Toyota Conference Integrated Micro Motion Systems: Mircomachining, Control and Application,* Nissin, Aichi, Japan, October 1989, 22, pp. 1–21.

[35] Hunter, I.W., and Kearney, R.E. Dynamics of human ankle stiffness: variation with mean ankle torque. *J. Biomechanics, 15,* 1982, pp. 747–752.

[36] Hunter, I.W., Lafontaine, S., Hollerbach, J.M., and Hunter, P.J. Fast reversible NiTi fibers for use in microrobotics. *Proc. IEEE Workshop on Micro Electro Mechanical Systems,* January 30–February 2, 1991, Nara, Japan, pp. 166–170.

[37] Hunter, I.W., Lafontaine, S., Nielsen, P.M.F., Hunter, P.J., and Hollerbach, J.M. Manipulation and dynamic mechanical testing of microscopic objects using a tele-microrobot system. *IEEE Control Systems Magazine, 10,* no. 2, 1990, pp. 3–9.

[38] Huxley, A.F. *Reflections on Muscle.* Princeton University Press, New Jersey, 1980.

[39] Ikuta, K. Micro/miniature shape memory alloy actuatory. *Proc. IEEE Intl. Conf. Robotics and Automation,* Cincinnati, Ohio, May 13–18, 1990, pp. 2156–2161.

[40] Ikuta, K., Kawahara, A., and Yamazumi, S. Miniature cybernetic actuators using piezoelectric device. *Proc. IEEE Workshop*

on Micro Electro Mechanical Systems, Nara, Japan, January 30–February 2, 1991, pp. 131–136.

[41] Ikuta, K., Tsukamoto, M., and Hirose, S. Shape memory alloy servo actuator system with electric resistance feedback application to active endoscope. *Proc IEEE Intl. Conf. Robotics and Automation,* Philadelphia, 1988, pp. 427–430.

[42] Ikuta, K., Tsukamoto, M., and Hirose, S. Mathematical model and experimental verification of shape memory alloy for designing micro actuator. *Proc. IEEE Workshop on Micro Electro Mechanical Systems,* Nara, Japan, January 30–February 2, 1991, pp. 103–108.

[43] Ilic-Spong, M., Marino, R., Peresada, S.M., and Taylor, D.G. Feedback linearizing control of switched reluctance motors. *IEEE Trans. Power Electronics, AC-32,* 1987, pp. 371–379.

[44] Immega, G.B. ROMAC actuators for micro robots. *Proc. IEEE Micro Robots and Teleoperators Workshop,* Hyannis, Massachusetts, 1987.

[45] Inoue, K. Rubbertuators and applications for robots. *Robotics Research: the 4th International Symposium,* R. Bolles and B. Roth, eds., MIT Press, Cambridge, Massachusetts, 1988, pp. 57–63.

[46] Jacobsen, S.C., Iversen, E.K., Knutti, D.F., Johnson, R.T., and Biggers, K.B. Design of the Utah/MIT Dexterous Hand. *Proc. IEEE Int. Conf. Robotics and Automation,* San Francisco, April 7–10, 1986, pp. 1520–1532.

[47] Jacobsen, S.C., Knutti, D.F., Biggers, K.B., Iversen, E.K., and Wood, D.F. An electropneumatic actuation system for the Utah/M.I.T. dexterous hand. *Theory and Practice of Robots and Manipulators. Proceedings of RoManSy '84: the Fifth CISM-IFToMM Symposium,* A. Morecki, G. Bianchi, and K. Kedzior, eds., MIT Press, Cambridge, Massachusetts, 1985, pp. 271–280.

[48] Jacobsen, S.C., Smith, C.C., Biggers, K.B., and Iversen, E.K. Behavior-based design for robot effectors. *Robotics Science,* edited by M. Brady, MIT Press, Cambridge, Massachusetts, 1989, pp. 505–539.

[49] Jacobsen, S.C., Smith, F.M., Backman, D.K., and Iversen, E.K. High performance, high dexteriy, force reflective teleoperator II. *ANS Topical Meeting on Robotics and Remote Systems,* Albuquerque, New Mexico, February 24–27, 1991.

[50] Jacobsen, S.C., Wood, J.E., Knutti, D.F., and Biggers, K.B. The Utah/MIT dexterous hand: work in progress. *Int. J. Robotics Research, 3* no. 4, 1984, pp. 21–50.

[51] Jiang, Z.W., Chonan, S., Abe, H., and Tani, J. Position control of a flexible arm using piezoelectric bimorph cells. *J. Dynamic Systems, Meas., Control, 113,* 1991, pp. 327–329.

[52] Kanade, T., and Schmitz, D. Development of the CMU Direct Drive Arm II. *Proc. American Control Conf.*, Boston, June 19–21, 1985, pp. 703–709.

[53] Kawamura, S., Miyata, K., Hanafusa, H., and Isida, K. PI type hierarchical feedback control scheme for pneumatic robots. *Proc. IEEE Int. Conf. Robotics and Automation,* Scottsdale, Arizona, May 14–19, 1989, pp. 1853–1858.

[54] Kazerooni, H., and Kim, S. A new architecture for direct drive robots. *Proc. IEEE Int. Conf. Robotics and Automation,* Philadelphia, April 24–29, 1988, pp. 442–445.

[55] Kearney, R.E., Hunter, I.W., Weiss, P.L., and Spring, K. Tilt-table/ankle-actuator system for the study of vestibulospinal reflexes. *Med. and Biol. Eng. and Comput., 21,* 1983, pp. 301–305.

[56] Kiesewetter, L. The application of Terfenol in linear motors. *Proc. 2nd Intl. Conf. Giant Magnetostrictive and Amorphous Alloys for Sensors and Applications,* 1988, pp. 1–18.

[57] Kishi, R., and Osada, Y. Reversible volume change of microparticles in an electric field. *J. Chemical Society, Faraday Transactions 1, 85,* 1989, pp. 655–662.

[58] Korane, K.J. Dispelling motion-control myths. *Machine Design,* October 11, 1990, pp. 52–56.

[59] Kuribayashi, K. Improvement of the response of an SMA actuator using a temperature sensor. *Intl. J. Robotics Research, 10,* 1991, pp. 13–20.

[60] Kuribayashi, K., and Yoshitake, M. Reversible SMA actuator for micro sized robot. *Proc. IEEE Workshop on Micro Electro Mechanical Systems,* Napa Valley, California, February 11–14, 1990, pp. 217–221.

[61] Kuwahara, H., Ono, Y., Nikaido, M., and Matsumoto, T. Development of high torque/precision servo system for direct-drive manipulator. *Robotics Research: The Third International Symposium,* edited by O. Faugeras and G. Giralt, MIT Press, Cambridge, Massachusetts, 1986, pp. 297–306.

[62] Lai, J.-Y., Menq, C.-H., and Singh, R. Accurate position control of a pneumatic actuator. *J. Dynamic Systems, Meas., Control, 112,* 1990, pp. 734–739.

[63] Laithwaite, E.R. Linear electric machines: a personal view. *Proc. IEEE, 63,* 1975, pp. 250–290.

[64] Lee, K.M., and Arjunan, S. A three degree of freedom micromotion in-parallel actuated manipulator. *Proc. IEEE Int. Conf. Robotics and Automation,* Scottsdale, Arizona, May 14–19, 1989, pp. 1698–1703.

[65] Lawrenson, P.J. *et al.* Variable speed switched reluctance motors. *IEE Proc.,* Vol. 127, Part B, no. 4, 1980.

[66] Leonhard, W. Adjustable-speed ac drives. *Proc. IEEE, 76,* 1988, pp. 455–471.

[67] Lin, S.J., and Akers, A. Dynamic analysis of a flapper-nozzle valve. *J. Dynamic Systems, Meas., Control, 113,* 1991, pp. 163–167.

[68] Liu, S., and Bobrow, J.E. An analysis of a pneumatic servo system and its application to a computer-controlled robot. *J. Dynamic Systems, Meas. and Control, 110,* 1988, pp. 228–235.

[69] Mannetje, J.J. Pneumatic servo design method improves system bandwidth twenty-fold. *Control Engineering,* June 1981, pp. 79–83.

[70] Maskrey, R.H., and Thayer, W.J. A brief history of electrohydraulic servomechanisms. *ASME J. Dynamic Systems, Meas., Control,* June 1978, pp. 110–116.

[71] Matsuda, R., and Kaneko, R. Micro-step xy-stage using piezoelectric tube actuator. *Proc. IEEE Workshop on Micro Electro Mechanical Systems,* Nara, Japan, January 30–February 2, 1991, pp. 137–142.

[72] McCormick, P.G. On the practical efficiency of shape memory engines. *Scripta Metallurgica, 21,* 1987, pp. 99–101.

[73] McLain, T.W., Iversen, E.K., Davis, C.C., and Jacobsen, S.C. Development, simulation, and validation of a highly nonlinear hydraulic servosystem model. *Proc. American Control Conf.*, Pittsburgh, June 21–23, 1989, pp. 385–391.

[74] Nakanishi, Y. Hydraulic actuators. *Actuators for Control,* edited by H. Funakubo, Gordon and Breach Science Publ., New York, 1991, pp. 34–90.

[75] Nakano, Y., Fujie, M., and Hosada, Y. Hitachi's robot hand. *Robotics Age, 6,* 1984, pp. 18–20.

[76] Niedermann, Ph., Emch, R., and Descouts, P. Simple piezoelectric translation device. *Reviews of Scientific Instruments, 59,* 1988, pp. 368–369.

[77] Ohno, E., and Sugimoto, K. Design and manufacture of dc motors for control. *Actuators for Control,* edited by H. Funakubo, Gordon and Breach Science Publ., New York, 1991, pp. 179–244.

[78] Osada, Y., Umezawa, K., and Yamauchi, A. Entrained responses of the current oscillation of polymer gels to sinusoidal stimulation. *Bull. Chemical Society of Japan, 62,* 1989, pp. 3232–3238.

[79] Pasch, K.A., and Seering, W.P. On the drive systems for high-performance machines. *J. Mechanisms, Transmissions, and Automation in Design, 106,*, 1984, pp. 102–108.

[80] Peterson, D.T., Verhoeven, J.D., McMasters, O.D., and Spitzig, W.A. Strength of Terfenol-D. *J. Applied Physics, 65,* 1989, pp. 3712–3713.

[81] Pugh, D.R., Ribble, E.A., Vohnout, V.J., Bihari, T.E., Walliser, T.M., Patterson, M.R., and Waldron, K.J. Technical description of the adaptive suspension vehicle. *Int. J. Robotics Research, 9* no. 2, 1990, pp. 24–42.

[82] Roberts, B.J. Poppet valves for directional control. *Machine Design,* August 11, 1988, pp. 119–122.

[83] Saito, Y. Pneumatic actuators. *Actuators for Control,* edited by H. Funakubo, Gordon and Breach Science Publ., New York, 1991, pp. 91–147.

[84] Say, M.G. *Alternating Current Machines,* Pitman Publishing Ltd., 1976, pp. 23–24.

[85] Suehiro, T., and Takase, K. Development of a direct-drive manipulator, ETA-3, and enhancement of servo stiffness by a second-order digital filter. *Proc. 15th Int. Symp. on Industrial Robots,* Tokyo, 1985, pp. 479–486.

[86] Suzuki, M. Amphoteric polyvinyl alcohol hydrogel and electrohydrodynamic control method for artificial muscles. *Polymer Gels,* D. DeRossi, ed., Plenum Press, New York, 1991, pp. 221–236.

[87] Suzumori, K., Iikura, S., and Tanaka, H. Flexible microactuator for miniature robots. *Proc. IEEE Workshop on Micro Electro Mechanical Systems,* Nara, Japan, January 30–February 2, 1991, pp. 204–209.

[88] Takahashi, S., Ochi, A., Yonezawa, M., Yano, T., Hamatsuki, T., and Fukui, I. Internal electrode piezoelectric ceramic actuator. *Ferroelectrics, 50,* 1983, pp. 181–190.

[89] Takase, K. Design of torque controlled manipulators composed of direct and low reduction ratio drive joints. *Robotics Research: The Third International Symposium,* edited by M. Brady and R. Paul, MIT Press, Cambridge, Massachusetts, 1984, pp. 655–675.

[90] Tatara, Y. Mechanochemical actuators. *Advanced Robotics, 2,* 1987, pp. 69–85.

[91] Taylor, D.G. An experimental study on composite control switched reluctance motors. *IEEE Control Systems Magazine, 11* no. 2, 1991, pp. 31–36.

[92] Thayer, W.J. *Specification Standards for Electrohydraulic Flow Control Servovalves.* Technical Bulletin 117, Moog Inc., East Aurora, New York 14052, 1962.

[93] Thayer, W.J. *Transfer Functions for Moog Servovalves.* Technical Bulletin 103, Moog Inc., East Aurora, New York 14052, 1965.

[94] Thayer, W.J. Electropneumatic servoactuation: an alternative to hydraulics for some low power applications Technical Bulletin 151, Moog Inc., East Aurora, New York 14052, 1984.

[95] Trimmer, W., and Jebens, R. Actuators for micro robots. *Proc. IEEE Int. Conf. Robotics and Automation,* Scottsdale, Arizona, May 14–19, 1989, pp. 1547–1552.

[96] Tzou
polyr
and
1709.

[97] Tzou
vibra
sensi
Robo
pp. 1

[98] Uchi
Cera

[99] Uday
L.S.,
thin
Elect
1991,

[100] Umet
multi
Symp

[101] Visch
contr
tiona
Verla

[102] Wang
acter
Cont

[103] Wells
tion
mode
nati,

[104] Wooc
ics. I
Flori

[105] Yano
effect
in Ja

[96] Tzou, H.S. Development of a light-weight robot end-effector using polymeric piezoelectric bimorph. *Proc. IEEE Int. Conf. Robotics and Automation,* Scottsdale, Arizona, May 14–19, 1989, pp. 1704–1709.

[97] Tzou, H.S., Wan, G.C., and Tseng, C.I. Dynamics and distributed vibration controls of flexible manipulators: integrated distributed sensing and active piezoelectric actuator. *Proc. IEEE Int. Conf. Robotics and Automation,* Scottsdale, Arizona, May 14–19, 1989, pp. 1716–1725.

[98] Uchino, K. Electrostrictive actuators: materials and applications. *Ceramic Bulletin, 65,* 1986, pp. 647–652.

[99] Udayakumar, K.R., Bart, S.F., Flynn, A.M., Chen, J., Tavrow, L.S., Cross, L.E., Brooks, R.A., and Ehrlich, D.J. Ferroelectric thin film ultrasonic micromotors. *Proc. IEEE Workshop on Micro Electro Mechanical Systems,* Nara, Japan, January 30–February 2, 1991, pp. 109–113.

[100] Umetani, Y., and Suzuki, H. Piezo-electric micro-manipulator in multi-degrees of freedom with tactile sensibility. *Proc. 10th Int. Symp. on Industrial Robots,* Milan, March 5–7, 1980, pp. 571–579.

[101] Vischer, D., and Khatib, O. Design and development of torque-controlled joints. *Experimental Robotics 1 — The First International Symposium,* edited by V. Hayward and O. Khatib, Springer-Verlag, New York, 1990, pp. 271–286.

[102] Wang, Z.X., Jouaneh, M.K., and Dornfeld, D.A. Design and characterization of a linear motion piezoelectric microactuator. *IEEE Control Systems Magazine, 10* no. 2, 1990, pp. 10–15.

[103] Wells, D., Iversen, E., Davis, C., and Jacobsen, S. An investigation of hydraulic actuator performance trade-offs using a generic model. *Proc. IEEE Intl. Conf. Robotics and Automation,* Cincinnati, Ohio, May 13–18, 1990, pp. 2168–2173.

[104] Woodson, H.H., and Melcher, J.R. *Electromechanical Dynamics. Part I: Discrete Systems,* R.E. Krieger Publ. Co., Malabar, Florida, 1990.

[105] Yano, T., and Takahashi, S. Utilization of piezoelectric stiffened effects on impact printer heads. *Electronics and Communications in Japan Part 2, 72* no. 10, 1989, pp. 19–32.

[106] Yano, T., Sato, E., Fukui, I., and Hori, S. Piezoelectric impact printhead utilizing longitudinal piezoelectric effect. *SID 89 Digest,* 1989, pp. 180–183.

[107] Youcef-Toumi, K., and Nagano, H. Design and control of drive systems using low reduction gears for force control. *Modeling and Control of Robotic Manipulators and Manufacturing Processes, DSC-Vol. 6,* ASME Winter Annual Meeting, Boston, Massachusetts, December 13–18, 1987, pp. 185–192.

[108] Xu, Y., Hunter, I.W., Hollerbach, J.M., and Bennett, D.J. An air-jet actuator system for identification of the human arm joint mechanical properties. *IEEE Trans. Biomedical Engineering,* 1991, in press.